The Cryosphere Discuss., 7, 1–34, 2013
www.the-cryosphere-discuss.net/7/1/2013/
doi:10.5194/tcd-7-1-2013

The Cryosphere Discussions

Spatial and temporal variations of glacier extent across the Southern Patagonian Icefield since the 1970s

A. White and L. Copland

Department of Geography, University of Ottawa, Ottawa, Ontario, Canada

Received: 10 July 2012 – Accepted: 28 November 2012 – Published: 2 January 2013

Correspondence to: A. White (awhit059@uottawa.ca)

Published by Copernicus Publications on behalf of the European Geosciences Union.

Abstract

A combination of Landsat and ASTER satellite scenes, from the 1970s to late-2000s, were used to quantify changes in the extent of glaciers in 130 basins across the Southern Patagonian Icefield (SPI). There was extensive net overall loss, with a reduction in ice area of ~ 420 km^2 (~ 3 % of the SPI) between 1984/86 and 2008/10. For glaciers which retreated, the mean annual loss rate was 0.19 km^2 yr^{-1} between 1976/79 and 1984/86, 0.16 km^2 yr^{-1} between 1984/86 and 2000/02, and 0.16 km^2 yr^{-1} between 2000/02 and 2008/10. Since the 1980s, glaciers located in the northwest quadrant of the SPI experienced the highest mean annual loss rates, at 0.22 km^2 yr^{-1}, while those in the southwest experienced the lowest mean annual loss rates, at 0.06 km^2 yr^{-1}. NCEP/NCAR climate reanalysis indicates that mean monthly surface air temperatures have increased by an average of +0.12 °C decade^{-1} (p = 0.0002) since 1950, particularly during the winter season, resulting in a change from mean negative to mean positive monthly winter temperatures and the earlier onset of spring. Increased winter temperatures have likely caused a switch in precipitation type from snow to rain and an associated reduction in glacier mass balance, even though there has been no significant trend in total annual precipitation over this period.

1 Introduction

The Southern Patagonian Icefield (SPI), also known as Hielo Patagónico Sur, is the largest temperate ice mass in the Southern Hemisphere. Located along the border between Chile and Argentina, it is ~ 350 km long, has an area of 13 000 km^2, and covers elevations up to 1500 m above sea level (a.s.l.) (Aniya et al., 1997; Naruse and Aniya, 1992) (Fig. 1). Outlet glaciers flow from the icefield in all directions, although the majority typically flow either westward into fjords or eastwards into lakes. Ice thicknesses at the floating fronts of several SPI glaciers (Tyndall, Grey, Moreno, Pio XI and Upsala) have been estimated to be 200 to 400 m thick (Aniya, 1999; Casassa, 1992;

Nichols and Miller, 1952; Warren, 1994; Warren and Rivera, 1994; Warren et al., 1995). Previous studies have used airborne and satellite imagery to inventory both the characteristics of SPI outlet glaciers (Aniya et al., 1996), as well as examine changes in their area, elevation, length and volume on both regional (Aniya et al., 1997; Aniya, 1999; Chen et al., 2007; López et al., 2010) and sub-regional scales (Rivera and Casassa, 2004).

The studies published in the 1990s by Aniya and co-workers examined the retreat rates of 48 SPI outlet glaciers between 1944/45 and 1986. Aniya et al. (1992) reported a general retreat, with Aniya (1999) stating that this comprised an areal loss of 202 km^2 for the 48 outlet glaciers and, an average retreat rate of 0.192 $km^2\,yr^{-1}$ for the 33 retreating outlet glaciers. The exception to this pattern was the Pio XI Glacier, where the net area increased over this period despite a retreat of its southern tongue (Aniya et al., 1992). In terms of spatial variability, glaciers north of 50° S had the greatest retreat rates (0.126 $km^2\,yr^{-1}$), particularly in the northwest (0.110 $km^2\,yr^{-1}$) (Aniya et al., 1997; Aniya, 1999). The lowest retreat rates were in the south (0.083 $km^2\,yr^{-1}$), with the southwest experiencing the lowest retreat at a rate of $< 0.020\,km^2\,yr^{-1}$. The eastern side of the icefield had higher and more variable retreat rates (0.141 $km^2\,yr^{-1}$) than the western side (0.115 $km^2\,yr^{-1}$). Strongly contrasting behaviours were sometimes observed between neighbouring glaciers on the east and west sides of the SPI. For example, the O'Higgins glacier had the highest total retreat (11 km) of any glacier on the eastern side of the SPI between 1945 and 1976, whereas the adjacent Pio XI glacier had the highest advance (9 km) of any glacier on the western side of the icefield over this period (Aniya et al., 1992). This was also observed from 1944/45 to 1986, where the Pio XI gained an area of 60 km^2 while the O'Higgins lost an area of $\sim 50\,km^2$ (Aniya, 1999).

Based on thickness data for five glaciers, Aniya (1999) estimated overall thinning rates of 1–3 $m\,yr^{-1}$ in the ablation zone of the SPI from 1944/45 to 1986, which would account for a total ice loss of 100–300 km^3 from the 2452 km^2 ablation area of the icefield over this period (excluding Pio XI and Perito Moreno glaciers). If this thinning

rate is also applied to the 7083 km^2 accumulation area, Aniya (1999) calculated a total volume loss of 285–670 km^3 from the SPI between 1944/45 and 1986.

In the southeastern portion of the SPI, Rivera and Casassa (2004) compared DEM, GPS, and optical survey data to reveal an 8 % total areal loss from 1945 to 2000, with strong thinning in the ablation zone of most glaciers from 1945 to 1995, but little evidence for change in the upper accumulation areas. Similar thinning patterns were observed by Keller et al. (2007) for the Tyndall Glacier (located in the southern region of the SPI), where thinning increased with decreasing altitude: $-7.7 \pm 1.0\,m\,yr^{-1}$ in the ablation zone compared to -1.0 to $-2.0 \pm 1.0\,m\,yr^{-1}$ near the equilibrium line at 900 m a.s.l. Recent observations of thinning (from 2000 to 2012) by Willis et al. (2012b) indicate that losses now extend to the highest elevations for most of the icefield, and predominantly across the large eastern glaciers. The observed thinning and retreat over the past century have been linked to both atmospheric warming and glacier dynamics, in part due to high thinning rates causing an increase in the buoyancy of glacier tongues and resulting increased flow rates and calving from longitudinal stretching (Rignot et al., 2003; Rivera and Casassa, 2004). The rate of retreat may also be controlled by the presence of debris cover in the ablation area, which can insulate the ice, prevent melt and stabilize the glacier front (Rivera and Casassa, 2004).

The contribution of recent SPI changes to sea level rise was examined by Rignot et al. (2003). Volume changes between 1968/1975–2000 were derived by comparing Shuttle Radar Topography Mission (SRTM) digital elevation data from 2000 to early cartography. For the largest 63 glaciers from 1968/75 to 2000, the icefield lost mass at a global sea level equivalent rate of $0.042 \pm 0.002\,mm\,yr^{-1}$. This rate more than doubled over 1995–2000 to $0.105 \pm 0.011\,mm\,yr^{-1}$, which likely made the SPI the highest cryospheric contributor to sea level rise outside of the ice sheets during this period. Using GRACE satellite data, Chen et al. (2007) found that the entire Patagonia Icefield (i.e. south and north combined) lost mass at a rate of $27.9 \pm 11\,km^3\,yr^{-1}$ over the period 2002–2006, equivalent to a global sea level rise of $0.078 \pm 0.031\,mm\,yr^{-1}$.

A common limitation with the studies described above is that they have relied on measurements taken from only the largest glaciers, or from the entire region at once. This limits understanding of local variability across the SPI, and means that a complete inventory of area changes across the icefield has not yet been completed. This study uses satellite imagery to quantify changes in the extent of the ablation zone of 93.5 % of glacier basins (or ∼ 98 % of the total glaciated area) across the SPI since the mid- to late-1970s. By including both large and small ice masses, this provides the most comprehensive quantification to date of glacier area changes across this region. Measurements are also updated to the year 2010, and NCEP/NCAR climate reanalysis is used to understand potential causes of the observed changes.

2 Data and methods

Changes in the extent of the ablation zone for each glacier basin were determined from optical satellite imagery that fell within the periods 1976–79, 1984–86, 2000–02 and 2008–10. These periods were selected based on the availability of cloud-free satellite imagery; only 9 glacier basins were excluded from analysis due to lack of image data or the basin being too small to delineate accurately. Changes in the accumulation area were not analyzed due to the frequent presence of snow cover at high altitudes that made it impossible to accurately identify the outline of nunataks in this region. This approach is consistent with previous studies of the SPI which have either not analyzed areal or thickness changes in the accumulation area (e.g. Aniya et al., 1992, 1997; Aniya, 1999; López et al., 2010), or have found little (Rignot et al., 2003; Rivera et al., 2005) to no significant change there (Rivera and Casassa, 2004). To analyse the spatial distribution of changes in glacier extent the icefield was divided into northeast, southeast, southwest, and northwest quadrants (Fig. 1).

2.1 Basin boundaries

The SPI was initially divided into drainage basins provided by the Laboratorio de Glaciologia at the Centro de Estudios Científicos, Valdivia, Chile (F. Bown, personal communication, 2010) as part of the Global Land Ice Measurements from Space project. The delineation of these polygons was verified and updated against Shuttle Radar Topography Mission (SRTM) elevation data with a resolution of 3 Arc Seconds (∼ 90 m), acquired from 11–22 February 2002. The SRTM data were obtained from the United States Geological Survey (USGS), and a polygon shapefile was delineated for each drainage basin by using the Basin tool in ESRI ArcMap 9.3. To create the basins, sinks were filled, and a D8 flow model was used to determine flow direction.

2.2 Glacier outlines

An outline of the ablation area of each glacier basin was digitized from orthorectified Landsat satellite imagery for each of the four time periods: 1970s, 1980s, early 2000s and late 2000s (Table 1). Images acquired during the summer were preferentially chosen with minimal cloud- and snow-cover to facilitate clear delineation of glacier extents. The Landsat images acquired on 14 January 1985 (60 m resolution) provide a complete view of the SPI in one day and were mosaicked and used as the master image against which all other satellite imagery was georectified. To georectify other images to this master mosaic, 20 to 70 ground control points (GCPs) were selected on each image in ESRI ArcMap 9.3 and a 3rd order polynomial transformation was applied. GCPs were chosen over flat, stable areas such as bedrock, and the final root mean square error for each georectified scene was less than its resolution (Table 1). While this type of coregistration may lead to errors over steep terrain, area measurements were focused across the ablation area, which typically has low surface slopes, and therefore would be less impacted by errors in this process.

To delineate between ice and surrounding bedrock the Landsat imagery was viewed as a false colour composite for processing. Landsat MSS scenes were represented

with bands 8, 5 and 4 placed in the red, green and blue channels (RGB), while Landsat TM and ETM+ scenes were represented with bands 7, 4 and 2 in the RGB channels. Other bands such as the thermal and 15 m panchromatic band (on the ETM+ sensor) were also used to refine the ice outlines. Due to a failure of the Landsat 7 scan line corrector, data gaps appear in post-2003 ETM+ imagery as striping (NASA, 2011). In areas where this affected determination of a glacier outline, the original image was superimposed over a Landsat scene acquired within a year of the original to fill any gaps. The actual dates of image acquisition were used to calculate annual retreat rates. If more than one image was used to conduct a measurement, the date from the image with the greater spatial coverage was used.

One ASTER image from 16 February 2010 (Table 1) was used to compensate for missing Landsat coverage of the west side of the SPI in the most recent time period. This image, selected from the TerraLook ASTER collection, was downloaded from the GLOVIS website (http://glovis.usgs.gov) and georectified against the 1986 Landsat mosaic using the methodology described above.

The region of each glacier analyzed in this study consists of the lower portion which could be clearly delineated in all images of each basin. These outlines typically correspond to the ablation area, although they may not necessarily cover the entire ablation zone in situations where the snow cover occurred at low elevations in the imagery. The basin outline for any areas above this region were kept constant for all time periods, and were based on the basin boundaries described in Sect. 2.1. A number of glaciers in the SPI have nunataks in their lower ablation areas which have become no longer surrounded by ice as their termini have retreated. In these cases the original nunatak area was subtracted from the ice area to prevent underestimation of ice loss.

All of the data concerning glacier extents was organized into a database by glacier name. These names were obtained from Aniya (1999) and from maps published by Zagier and Urruty (2010) and Chaltén Out Door maps (2010). For glaciers where a name could not be found, an ID number was assigned to the glacier as "U" (unnamed) followed by a number (starting at 1). Glaciers were defined as stationary when

they experienced a change in total area of $< 0.0036\,km^2$ (the size of a single cell in Landsat MSS imagery) between measurement periods.

2.3 Error analysis

To calculate the uncertainty in our area change calculations we used the method outlined by Hall et al. (2003). First, the uncertainty of the change in terminus position in the linear dimension (d) between two satellite images was evaluated by using the formula (after Williams et al., 1997):

$$d = \sqrt{r_1^2 + r_2^2} + \mathrm{RMSE} \quad (1)$$

where r_1 represents the cell size of the first image, r_2 the cell size of the second image, and RMSE the error determined during the georectification process (Table 1). To evaluate the worst-case value for uncertainty we used the largest cell size in our study for r_1 and r_2 (60 m), and the highest RMSE value (34.08 m) to produce a value for d of 118.93 m. To convert this linear uncertainty into an estimation of uncertainty in area change (a), the following equation was used (Hall et al., 2003):

$$a = A \cdot (2d/x) \quad (2)$$

where $A = x^2$, with x = linear side dimension (60 m for MSS data). For our study this produces a maximum uncertainty in area change of $\pm 0.014\,km^2$, and considerably less than this for imagery with a resolution of 15 or 30 m.

Errors may also arise as a result of misinterpretation of the glacier extent due to factors such as snow or debris cover. To minimize the interference of snow cover during the delineation process, only images with minimal snow cover were used, typically from late summer. Furthermore, the fact that this study only evaluates changes in the lower elevation, ablation area of glaciers also minimizes the influence of snow cover. In the case of debris-covered glaciers, one of two methods was used to delineate the

edge of the terminus. If flow lines were visible on a debris-covered glacier surface (e.g. medial moraines), these served as a guide for tracing the terminus. If, however, evidence of motion could not be seen on the surface, then the extent was determined as the edge of ice not covered by debris. Whichever method was selected for the first year of measurement, it was kept consistent to analyze the other years for each glacier basin.

2.4 Climate data

To examine climate variability since 1950, NCEP/NCAR Reanalysis monthly mean data was downloaded from the NOAA Earth System Research Laboratory website (http://www.esrl.noaa.gov/psd/data/reanalysis/reanalysis.shtml). This data is drawn from an assimilated gridded (2.5° × 2.5° grid) dataset, based on observations from meteorological stations with a numerical weather prediction model (Kalnay et al., 1996). For this study, mean monthly surface (2 m above surface) air temperatures and total precipitable water from 1950 to 2010 were analyzed for grid cells centered on the northern and southern halves of the SPI (Fig. 1 inset). These variables were chosen based on the results of Cook et al. (2003), who showed that winter and summer precipitation, as well as summer temperatures, are the main determinants of glacier mass balance on the SPI. To calculate positive degree days (PDD) and freezing degree days (FDD) the mean monthly temperature was multiplied by the number of days in each month.

3 Results

Measured changes in the area of an ablation zone occurred due to: (1) changes in position of a glacier terminus, and/or (2) narrowing of a glacier trunk and tributary branches. In general, there was a widespread decrease in areal extent for almost all glaciers over the period of study (Tables 2 and 3, Figs. 2 and 3). From the 1970s to 1980s, 97/100 glaciers lost area, while three experienced a gain. During this first

period, 30 glaciers had to be excluded due to lack of cloud-free imagery. From the 1980s to the 2000s, 114/130 glaciers lost area, and 16 showed advance. From the early to late 2000s, 115/130 glaciers retreated, 12 showed advance, and three showed no discernible change. Note that mean annual retreat rates provided below include all glacier changes whether they were advance, stationary, or retreat, unless otherwise stated.

3.1 Glacier changes of the eastern SPI

A total of 52 glacier basins were measured on the eastern side of the SPI (Table 2). From the 1970s to the late 2000s all glaciers experienced some ice loss, with the greatest loss rate of 2.33 $km^2\,yr^{-1}$ on the Upsala Glacier from the 1970s to late 2000s (Fig. 4a). Broken down by period, 100 % of glaciers retreated between 1976/79 and 1984/86. The highest loss rates occurred from the Upsala, O'Higgins and Dickson/Cubo glaciers during this period, with rates of 2.56 $km^2\,yr^{-1}$, 1.23 $km^2\,yr^{-1}$ and 0.80 $km^2\,yr^{-1}$, respectively.

Over the 1984/86 to 2000/02 period, 94.2 % of glaciers retreated, while 5.8 % advanced. The U1 Glacier had the greatest advance by a total of only 0.14 km^2 (0.008 $km^2\,yr^{-1}$). The highest retreat rates during the second period were from the Upsala, Tyndall, Grey and Lucia glaciers with rates ranging from 0.52 to 2.16 $km^2\,yr^{-1}$.

The third period of study (2000/02 to 2008/10) revealed that 88.5 % of glaciers retreated, while 3.9 % were stationary and 7.7 % advanced. The Perito Moreno Glacier (Fig. 4b) expanded by 0.61 km^2 at a mean annual rate of 0.08 $km^2\,yr^{-1}$. The highest retreat rates were observed from the Viedma, Tyndall, and Upsala glaciers with rates of 0.65 to 2.50 $km^2\,yr^{-1}$.

3.2 Glacier changes of the western SPI

Area fluctuations for the 78 glaciers measured on the west side of the SPI were generally more variable than those on the east side. The Jorge Montt Glacier (Fig. 5a)

had the greatest decrease in area with a total ice loss of 53.75 km^2 from the 1970s to the late 2000s, at a mean annual rate of 1.58 $km^2\,yr^{-1}$. The Occidental, Bernardo and Greve glaciers also had high total areal retreats of 23.02 km^2, 28.28 km^2, and 32.20 km^2, at rates of 0.68 $km^2\,yr^{-1}$, 0.86 $km^2\,yr^{-1}$, and 0.95 $km^2\,yr^{-1}$, respectively. Approximately 21 % of glaciers showed expansion in area during at least one of the three time periods examined. The greatest total expansion occurred on Pio XI Glacier, which increased in area at a rate of 0.53 $km^2\,yr^{-1}$ for a total of 18.19 km^2 from the 1970s to the late 2000s (Fig. 5b).

Of the 49 glaciers measured between 1976/79 and 1984/86, 46 showed retreat and 3 advanced (Table 3). Due to the lack of clear satellite imagery, 29 glacier basins were excluded from this first period of study. The Pio XI and U13 glaciers demonstrated an expansion of 4.70 km^2 (from 25 February 1976 to 14 January 1986) and 0.47 km^2 (from 08 March 1979 to 14 January 1986) at rates of 0.47 and 0.07 $km^2\,yr^{-1}$, respectively. The Greve, Occidental, and Tempano glaciers had the highest rates of retreat ranging from 0.52 to 0.88 $km^2\,yr^{-1}$.

Between 1984/86 and 2000/02, 65 glaciers retreated and 13 advanced. The highest rates of advance were measured on the Pio XI (0.53 $km^2\,yr^{-1}$) and U13 (0.16 $km^2\,yr^{-1}$) glaciers. The highest rates of retreat were observed from the HPS-38, Greve, Bernardo, and Jorge Montt glaciers with rates ranging from 0.59 to 2.77 $km^2\,yr^{-1}$.

Between 2000/02 and 2008/10, 68 glaciers retreated, 1 remained stationary, and 9 advanced. The highest rates of expansion were once again observed on the Pio XI and U13 glaciers (0.62 $km^2\,yr^{-1}$ and 0.08 $km^2\,yr^{-1}$, respectively). During this period the highest retreat rates occurred on the Tempano, HPS41, U92, Bernardo, HPS12, Greve, Occidental and Jorge Montt glaciers, with rates from 0.53 to 1.21 $km^2\,yr^{-1}$.

3.3 Spatial distribution of mean annual retreat rates

The spatial distribution of glacier retreat rates across the SPI showed marked variability (Figs. 6 and 7). In terms of the greatest differences, the northern glaciers showed

a mean annual retreat rate of 0.18 $km^2\,yr^{-1}$ between the 1970s and late-2000s compared to a mean retreat rate of 0.09 $km^2\,yr^{-1}$ for the southern glaciers. Based on an east-west division, glaciers on the eastern half of the icefield had higher mean annual retreat rates (0.17 $km^2\,yr^{-1}$) compared to glaciers on the western half (0.11 $km^2\,yr^{-1}$). Overall, glaciers in the north-west and north-east quadrants had the highest mean retreat rates of 0.19 $km^2\,yr^{-1}$ and 0.17 $km^2\,yr^{-1}$, respectively, whereas glaciers in the southwest had the lowest mean retreat rates of 0.06 $km^2\,yr^{-1}$ (Fig. 6d).

Broken down by individual period, the distribution of mean annual retreat rates was not consistent, although the southwest remained the quadrant with the lowest retreat rate throughout all three study periods. From 1976/79 to 1984/86 the highest retreat occurred in the southeast, followed by the northeast (Fig. 6a). During the second period (1984/86 to 2000/02) the highest retreat rates occurred in the northwest, followed by the northeast (Fig. 6b). From 2000/02 to 2008/10, the highest rates of retreat were found in the northwest, followed by the northeast and southeast (Fig. 6c).

3.4 Climate analysis

Our climate reanalysis indicates that over the past six decades the northern and southern halves of the SPI have warmed by 0.13 °C $decade^{-1}$ ($p = 0.0003$) and 0.12 °C $decade^{-1}$ ($p = 0.0001$), respectively. Seasonally, autumn (March, April, May) has shown the greatest increase in mean monthly surface air temperature by 0.13 °C $decade^{-1}$ ($p = 0.0048$), followed by summer (December, January, February) and spring (September, October, November) at 0.08 °C $decade^{-1}$ ($p = 0.1116$ and $p = 0.0337$, respectively). Winter (June, July, August) has shown the weakest rate of warming at 0.02 °C $decade^{-1}$ ($p = 0.00005$), although there has been a marked regime shift over this period with decadal surface air temperatures indicating a switch from mean negative to mean positive monthly winter temperatures in the northern half of the SPI (Fig. 8). In both the northern and southern halves of the SPI winter temperatures

were at their lowest in the 1950s, increased but remained relatively consistent throughout the 1960s–1990s, and increased again in the 2000s.

4 Discussion

This study indicates that glacier area losses are widespread and continuing across the SPI, although there is marked spatial variability. These patterns are consistent with those observed by Rignot et al. (2003) over the period 1968/1975–2000, where glaciers on the northern half of the SPI thinned more rapidly than glaciers on the southern half. Similarly, for the 1940s–1990s, Aniya et al. (1997) reported higher retreat rates in the north compared to the south, and higher retreat rates in the east compared to the west, resulting in lowest overall retreat rates in the southwest and largest in the northwest. In our study we observed major retreats in the north, compared to the south where length changes were typically < 2 km. López et al. (2010) studied the length fluctuations of 32 glaciers across the SPI over the period 1945–2005 and also reported glacier retreats < 2 km in the southern portion of the icefield, with an exception of the southernmost part where glaciers were reported to have retreated by > 2 km from 1945 to 2005. Although this was observed in the current study, it is also noted that the highest retreat rates in the southernmost portion of the SPI were almost exclusively limited to the east of side of the icefield (with the exception of HPS-41 Glacier).

During the period 1945–2005, López et al. (2010) observed an advance of the front of the Perito Moreno, HPS-19, and Pio XI glaciers. In this study, however, periods of retreat were more significant in the recent past, resulting in net losses for the HPS-19 and Perito Moreno glaciers over the 1970s to late 2000s. For example, HPS-19 showed a retreat from 1979 to 1985 of 0.53 km^2, but from 1985 to 2010 it advanced by 0.08 km^2. In comparison, López et al. (2010) based the HPS-19 advance on a single measurement to calculate a net frontal advance of 1.42 km between 1945 and 2000. We have recorded both advance and retreats of the Perito Moreno Glacier during our study periods, with a retreat of 3.23 km^2 from 1979 to 2002 and an advance of 0.61 km^2 from

2002 to 2010, resulting in a net area loss of 2.61 km^2. Again, López et al. (2010) measured a net loss in length of 0.64 km from single measurements at the start and end of the 1945–2000 period. These examples illustrate the importance of regular monitoring of glacier length and area variations to fully understand trends occurring across the SPI.

In our study the Pio XI glacier demonstrated an advance of 18.19 km^2 from the 1970s to the late 2000s, with a net increase through each time period. The looped moraines visible on the Pio XI terminus in the 1970s and 1980s suggest that the advance could be attributed to surging. Rivera et al. (1997a,b) proposed several explanations for this surging, including increased sliding caused by geothermal activity, enhanced basal water pressure, increased precipitation prior to surge events, and reduced calving as water depths decreased at the glacier front from sedimentation.

For the SPI as a whole, several studies have shown evidence for long-term regional warming. Based on surface air temperature data from 1933–1992, Rosenblüth et al. (1997) used a linear trend line to derive warming rates of 1.3–2.0 $^{\circ}C\,century^{-1}$ for Patagonia, although a cooling period occurred near 41° S from the 1950s to the 1970s. In a study by Ibarzábal y Donángelo et al. (1996), temperature and precipitation observations from four stations located to the east and northeast (47–52° S) of the SPI showed stronger warming and decreasing annual precipitation towards the south (at Lago Argentino) over the past 50 to 60 yr.

From the above review it is clear that the climate of the SPI warmed throughout most of the 20th century. Our NCEP/NCAR reanalysis of mean monthly surface air temperatures indicates that fundamental changes are continuing in the Patagonian climate. This is particularly true in the winter, with the first decade of the 21st century being markedly warmer than any previous decade in both the northern and southern areas of the SPI. Over the entire period of study (1950 to 2010) the mean annual surface air temperature increased by 0.77 °C in the northern half, compared to 0.73 °C in the southern half. The net result of these changes has been the later onset of winter and earlier onset of spring across the SPI, resulting in an overall lengthening of the

melt season. This has implications for precipitation type as the snow to precipitation (S/P) ratio will decrease as more winter precipitation events occur as rain in a warming climate. Analysis of precipitation patterns across the icefield indicates little change in total precipitation amount since the 1950s, but a reduction in the S/P ratio would still result in a decrease in annual snow accumulation and an increase in energy for melt from rain on the glacier surface.

Aside from climate changes, local changes in glacier dynamics may also play an important role in controlling the observed area losses. For example, Rivera and Casassa (2004) argue that surface ablation rates calculated from field measurements and a degree day model are insufficient to account for all of the observed thinning rates observed on the terminus of the Perito Moreno Glacier. Instead, they argue that glacier dynamics must play a significant role, particularly on glaciers that terminate in water. Venteris (1999) argues that rapid retreat of grounded calving glaciers in Patagonia is primarily caused by the thinning and near-flotation of the terminus, and further weakened by basal crevassing, which is itself caused by longitudinal stretching and rapid calving. The role of pinning points can also be an important consideration, with an increase in calving and retreat caused by the removal of backstress after a glacier retreats from a pinning point (e.g. island, terminal moraine shoal). For example, Cassasa et al. (1997) examined the recession of the O'Higgins Glacier over a century and found that it retreated rapidly into deeper water after it lost connection to Isla Chica after a period of warming between 1896 and 1914. This rapid retreat eventually decelerated, likely due to the retreat of the glacier into shallower waters. Similarly, the rapid recent retreat of the Upsala Glacier is likely related to a loss of terminus stability after it retreated past the Brazo Upsala islands (Skvarca et al., 2003).

In comparison with the Northern Patagonia Icefield (NPI), immediately north of the SPI, it is apparent that while both icefields are undergoing losses, there are differences in their thinning rates and spatial distribution of changes. Previous studies have indicated that over the period 1968/1975 to 2012, thinning at the SPI occurred well above the ELA, while thinning across the NPI was only observed up to the ELA (Rignot et al.,

2003; Willis et al., 2012a,b). Unlike the SPI, however, there is no evidence for advance or stationary status for glaciers on the NPI from 1945 to 2011, with all NPI glaciers retreating over this period (López et al., 2010; López and Casassa, 2011). According to observations of relative retreat rate for 15 glaciers from 1945 to 2005 analyzed by López et al. (2010) the changes across the NPI are more homogenous compared to the SPI, although highest losses across the NPI have been observed in the northwest (similar to the SPI) and the southwest (López and Casassa, 2011).

5 Conclusions

Of the 130 glacier basins measured across the SPI in this study, only the Pio XI and the U13 glaciers experienced a substantial increase in area. From the 1970s to the 1980s, 97 % of the glaciers lost area and 3 % advanced. From the 1980s to late 2000s, 90.8 % of glaciers retreated while 8.5 % advanced and 0.8 % remained static. Based on total basin size in the 1980s, smaller glaciers ($<\sim 100\,\mathrm{km}^2$) had much lower retreat rates for the entire study period, with an average areal change rate of $0.06\,\mathrm{km}^2\,\mathrm{yr}^{-1}$, whereas large glaciers ($>\sim 100\,\mathrm{km}^2$) changed area at an average rate of $0.37\,\mathrm{km}^2\,\mathrm{yr}^{-1}$. Over the three time periods, the rate of glacier change has decreased slightly recently; from the 1970s to the 1980s the mean retreat rate was $0.17\,\mathrm{km}^2\,\mathrm{yr}^{-1}$, from the 1980s to 2000s this was $0.14\,\mathrm{km}^2\,\mathrm{yr}^{-1}$, and from the early 2000s to late 2000s it was $0.13\,\mathrm{km}^2\,\mathrm{yr}^{-1}$. If only the glaciers which retreated are considered, the mean annual loss rate was $0.19\,\mathrm{km}^2\,\mathrm{yr}^{-1}$ between 1976/79 and 1984/86, $0.16\,\mathrm{km}^2\,\mathrm{yr}^{-1}$ between 1984/86 and 2000/02, and $0.16\,\mathrm{km}^2\,\mathrm{yr}^{-1}$ between 2000/02 and 2008/10. Overall change rates in the north have remained generally stable since the 1970s, however rates in the northwest have increased by 61.5 % between the 1970s and late-2000s. Since the 1970s, change rates decreased by 36 % in the southeast and 37.5 % in the southwest.

The widespread losses are likely due to negative mass balances linked to winter warming that has risen mean monthly winter temperatures from just below freezing to just above freezing in many regions. This has resulted in a lengthened melt season

and reduction in the proportion of total precipitation falling as snow. The significance of changes in precipitation form, even without changes in total precipitation, has recently been highlighted for locations such as the Arctic (Screen and Simmonds, 2011) and Switzerland (Serquet et al., 2011), but has not previously been reported for the SPI.

In the future, an improved network of weather stations and mass balance monitoring locations need to be installed along the SPI to confirm regional climate variations and trends in glacier mass balance. Case studies also need to be completed to investigate why some glaciers have displayed extremely high losses (e.g. Upsala), while others remain stationary. Additional factors such as the development of proglacial lakes, underlying topography, and the presence of debris-cover can have a strong influence on glaciers, and therefore further investigation of these are required to better understand the ice losses observed on the SPI.

Acknowledgements. We would like to thank Canada Foundation for Innovation, Ontario Research Fund, Natural Resources and Engineering Research Council of Canada, University of Ottawa and Natural Resources Canada for assistance with funding for this project. We also thank the members of the Laboratory for Cryospheric Research for their support and Derek Mueller for his helpful reviews of this paper.

References

Aniya, M.: Recent glacier variations of the Hielos Patagónicos, South America, and their contribution to sea-level change, Arct. Antarct. Alp. Res., 31, 165–173, 1999.

Aniya, M., Naruse, R., Shizukuishi, M., Skvarca, P., and Casassa, G.: Monitoring recent glacier variations in the Southern Patagonia Icefield, utilizing remote sensing data, Int. Arch. Photogramm. Remote Sens., 29, 87–94, 1992.

Aniya, M., Sato, H., Naruse, R., Skvarca, P., and Casassa, G.: The use of satellite and airborne imagery to inventory outlet glaciers of the Southern Patagonia Icefield, Photogramm. Eng. Remote Sens., 62, 1361–1369, 1996.

Aniya, M., Sato, H., Naruse, R., Skvarca, P., and Casassa, G.: Recent glacier variations in the Southern Patagonia Icefield, South America, Arct. Alp. Res., 29, 1–12, 1997.

Casassa, G.: Radio-echo sounding of Tyndall Glacier, southern Patagonia, Bull. Glacier Res., 10, 69–74, 1992.

Casassa, G., Brecher, H., Rivera, A., and Aniya, M.: A century-long recession record of Glaciar O'Higgins, Chilean Patagonia, Ann. Glaciol., 24, 106–110, 1997.

Chaltén Out Door Maps: Glacier Perito Moreno topographical map El Calafate, Chaltén Out Door Maps, El Chaltén, 2010.

Cook, K. H., Yang, X., Carter, C. M., and Belcher, B. N.: A modeling system for studying climate controls on mountain glaciers with application to the Patagonian Icefields, Climatic Change, 56, 339–367, 2003.

Hall, D. K., Bayr, K. J., Schöner, W., Bindschadler, R. A., and Chien, J. Y. L.: Consideration of the erros inherent in mapping historical glacier positions in Austria from the ground and space (1893–2001), Remote Sens. Environ., 86, 566–577, 2003.

Ibarzabal y Donangelo, T., Hoffmann, J. A., and Naruse, R.: Recent climate changes in southern Patagonia, Bull. Glacier Res., 14, 29–36, 1996.

Kalnay, E., Kanamitsu, M., Kistler, R., Collins, W., Deaven, D., Gandin, L., Iredell, M., Saha, S., White, G., Woolen, J., Zhu, Y., Chelliah, M., Ebisuzaki, W., Higgins, W., Janowiak, J., Mo, K. C., Ropelewski, C., Wang, J., Leetma, A., Reynolds, R., Jenne, R., and Joseph, D.: The NCEP/NCAR reanalysis 40-year project, B. Am. Meteorol. Soc., 77, 437–471, 1996.

Keller, K., Casassa, G., Rivera, A., Forsberg, R., and Gundestrup, N.: Airborne laser altimetry survey of Glaciar Tyndfall, Patagonia, Global Planet. Change, 59, 101–109, 2007.

López, P. and Casassa, G.: Recent acceleration of ice loss in the Northern Patagonia Icefield based on an updated decennial evolution, The Cryosphere Discuss., 5, 3323–3381, doi:10.5194/tcd-5-3323-2011, 2011.

López, P., Chevallier, P., Favier, V., Pouyaud, B., Ordenes, F., and Oerlemans, J.: A regional view of fluctuations in glacier length in southern South America, Global Planet. Change, 71, 85–108, 2010.

Naruse, R. and Aniya, M.: Outline of glacier research project in Patagonia, 1990, Bull. Glacier Res., 10, 31–38, 1992.

National Aeronautics and Space Administration (NASA): Landsat 7 Science Data Users Handbook, Chapter 11 – data products, availoable at: http://landsathandbook.gsfc.nasa.gov/data_prod/prog_sect11_3.html (last access: 20 December 2012), 2011.

Nichols, R. L. and Miller, M. M.: The Moreno Glacier, Lago Argentino, Patagonia: advancing glaciers and nearby simultaneously retreating glacier, J. Glaciol., 2, 41–46, 1952.

Rignot, E., Rivera, A., and Casassa, G.: Contribution of the Patagonia Icefields of South America to sea level rise, Science, 302, 434–437, 2003.
Rivera, A. and Casassa, G.: Ice elevation, areal, and frontal changes of glaciers from National Park Torres del Paine, Southern Patagonia Icefield, Arct. Antarct. Alp. Res., 36, 379–389, 2004.
Rivera, A., Aravena, J. C., and Casassa. G.: Recent fluctuations of Glaciar Pio XI, Patagonia: discussion of glacial surge hypothesis, Mt. Res. Dev., 17, 309–322, 1997a.
Rivera, A., Lange, H., Aravena, J. C., and Casassa, G.: The 20th-century advance of Glaciar Pio XI, Chilean Patagonia, Ann. Glaciol., 24, 66–71, 1997b.
Rivera, A., Casassa, G., Bamber, J., and Kääb, A.: Ice elevation changes of Glaciar Chico, southern Patagonia, using ASTER DEMs, aerial photographs and GPS data, J. Glaciol., 51, 105–112, 2005.
Rivera, A., Benham, T., Casassa, G., Bamber, J., and Dowdeswell, J.: Ice elevation and areal changes of glaciers from the Northern Patagonia icefield, Chile, Global Planet. Change, 59, 126–137, 2007.
Rosenblüth, B., Fuenzalida, H. A., and Aceituno, P.: Recent temperature variations in Southern South America, Int. J. Climatol., 17, 67–85, 1997.
Screen, J. A. and Simmonds, I.: Declining summer snowfall in the Arctic: causes, impacts and feedbacks, Clim. Dynam., 38, 2243–2256, doi:10.1007/s00382-011-1105-2, 2011.
Serquet, G., Marty, C., Dulex, J.-P., and Rebetez, M.: Seasonal trends and temperature dependence of the snowfall/precipitation-day ratio in Switzerland, Geophys. Res. Lett., 38, L07703, doi:10.1029/2011GL046976, 2011.
Skvarca, P., Raup, B., and De Angelis, H.: Recent behaviour of Glaciar Upsala, a fast-flowing calving glacier in Lago Argentino, southern Patagonia, Ann. Glaciol., 36, 184–188, 2003.
United States Geological Survey (USGS): EarthExplorer, available at: http://earthexplorer.usgs.gov/ (last access: 20 December 2012), 2012.
Venteris, E. R.: Rapid tidewater glacier retreat: a comparison between Columbia Glacier, Alaska and Patagonian calving glaciers, Global Planet. Change, 22, 131–138, 1999.
Warren, C. R.: Freshwater calving and anomalous glacier oscillations: recent behavior of Moreno and Ameghino glaciers, Patagonia, Holocene, 4, 422–429, 1994.
Warren, C. R. and Rivera, A.: Non-linear response of calving glaciers: a case study of Pio XI Glacier, Rev. Chil. Hist. Nat., 67, 385–394, 1994.

Warren, C. R., Greene, D. R., and Glasser, N. F.: Upsala Glacier, Patagonia: rapid calving retreat in freshwater, Ann. Glaciol., 21, 311–316, 1995.
Williams Jr., R. S., Hall, D. K., Sigurdsson, O., and Chien, J. Y. L.: Comparison of satellite-derived with ground-based measurements of the fluctuations of the margins of Vatnajökull, Iceland, 1973–92, Ann. Glaciol., 24, 72–80, 1997.
Willis, M. J., Melkonian, A. K., Pritchard, M. E., and Rivera, A.: Ice loss from the Southern Patagonian Ice Field, South America, between 2000 and 2012, Geophys. Res. Lett., 39, L17501, doi:10.1029/2012GL053136, 2012a.
Willis, M. J., Melkonian, A. K., Pritchard, M. E., and Ramage, J. M.: Ice loss rates at the Northern Patagonian Icefield derived using a decade of satellite remote sensing, Remote Sens. Environ., 117, 184–198, 2012b.
Zagier and Urruty: Patagonian South Icefield Trekking Map, Zagier and Urruty Publications, Buenos Aires, 2010.

Table 1. Satellite imagery used to measure glacier extents in this study. All Landsat images were obtained from the USGS Global Visualization Viewer (http://glovis.usgs.gov/).

Satellite	Sensor	Date	Image ID	Processing Level*	Resolution	Coverage	Number of GCPs	RMSE (m)
Landsat 2	MSS	25 Feb 1976	LM22480941976056AAA05	L1T	60 m	Northern	50	33.36
Landsat 2	MSS	4 May 1978	LM32460961978124AAA05	L1T	60 m	South-East	–	–
Landsat 2	MSS	2 Jan 1979	LM22460951979002AAA08	L1T	60 m	Moreno	–	–
Landsat 2	MSS	2 Jan 1979	LM22460961979002AAA04	L1T	60 m	South-East	–	–
Landsat 2	MSS	22 Jan 1979	LM22480941979022AAA04	L1G	60 m	Northern	–	–
Landsat 3	MSS	8 Mar 1979	LM32480941979067AAA03	L1G	60 m	Northern	40	34.08
Landsat 3	MSS	8 Mar 1979	LM32480951979067AAA03	L1G	60 m	Central	–	–
Landsat 5	MSS	26 Dec 1984	LM52310951984361AAA03	L1T	60 m	Central	–	–
Landsat 5	TM	27 Jan 1985	LT52310941985027AAA04	L1T	30 m	Northern	–	–
Landsat 5	TM	27 Jan 1985	LT52310951985027AAA03	L1T	30 m	Central	–	–
Landsat 5	MSS	14 Jan 1986	LM52310941986014AAA03	L1T	60 m	Northern	–	–
Landsat 5	MSS	14 Jan 1986	LM52310951986014AAA03	L1T	60 m	Central	–	–
Landsat 5	MSS	14 Jan 1986	LM52310961986014AAA03	L1T	60 m	Southern	–	–
Landsat 5	TM	4 Oct 1986	LT52320941986277XXX02	L1T	30 m	Northern	–	–
Landsat 5	TM	4 Oct 1986	LT52320951986277XXX02	L1T	30 m	Central-West	–	–
Landsat 5	MSS	9 Feb 1987	LM52320941987040AAA03	L1T	60 m	Northern	43	33.89
Landsat 7	ETM+	27 Oct 2000	LE72310952000301EDC00	L1T	30 m	Central	–	–
Landsat 7	ETM+	27 Oct 2000	LE72310962000301EDC00	L1T	30 m	Southern	–	–
Landsat 7	ETM+	20 Mar 2001	LE72310942001079EDC02	L1T	30 m	Northern	–	–
Landsat 7	ETM+	20 Mar 2001	LE72310962001079EDC02	L1T	30 m	Southern	–	–
Landsat 7	ETM+	20 Mar 2001	LE72310952001079EDC02	L1T	30 m	Central	–	–
Landsat 7	ETM+	7 May 2001	LE72310952001127EDC00	L1T	30 m	Central	–	–
Landsat 7	ETM+	7 May 2001	LE72310962001127EDC00	L1T	30 m	Southern	–	–
Landsat 7	ETM+	14 Oct 2001	LE72310942001287EDC00	L1T	30 m	Northern	–	–
Landsat 7	ETM+	18 Jan 2002	LE72310942002018EDC00	L1T	30 m	Northern	–	–
Landsat 7	ETM+	18 Jan 2002	LE72310952002018EDC00	L1T	30 m	Central	–	–
Landsat 7	ETM+	8 Apr 2002	LE72310952002098EDC00	L1T	30 m	Central	–	–
Landsat 7	ETM+	17 May 2002	LE72320942002137EDC00	L1T	30 m	Northern	–	–
Landsat 7	ETM+	11 Dec 2002	LE72320942002345PFS00	L1T	30 m	Northern	–	–
Landsat 7	ETM+	27 Feb 2005	LE72310952005058EDC00	L1T	30 m	Central	–	–
Landsat 7	ETM+	19 Jan 2008	LE72310952008019EDC00	L1T	30 m	Central	–	–
Landsat 7	ETM+	28 Jan 2008	LE72300962008028EDC00	L1T	30 m	Southern	–	–
Landsat 7	ETM+	12 Jan 2009	LE72320942009012EDC00	L1T	30 m	Northern	–	–
Landsat 7	ETM+	18 Sep 2009	LE72310952009261EDC00	L1T	30 m	Central	–	–
Landsat 7	ETM+	7 Dec 2009	LE72310942009341EDC00	L1T	30 m	Northern	–	–
Landsat 7	ETM+	7 Dec 2009	LE72310952009341EDC00	L1T	30 m	Central	–	–
Landsat 7	ETM+	24 Jan 2010	LE72310942010024EDC00	L1T	30 m	Northern	–	–
Landsat 7	ETM+	16 Feb 2010	LE72320942010047EDC00	L1T	30 m	Northern	–	–
Landsat 7	ETM+	16 Feb 2010	LE72320952010047EDC00	L1T	30 m	Central-West	–	–
Terra	ASTER	16 Feb 2010	AST_L1A.003:2078231791	L1A	15 m	Central-West	–	–
Landsat 7	ETM+	25 Feb 2010	LE72310942010056EDC00	L1T	30 m	Northern	–	–
Landsat 7	ETM+	25 Feb 2010	LE72310952010056EDC00	L1T	30 m	Central	–	–
Landsat 7	ETM+	4 Mar 2010	LE72320942010063EDC00	L1T	30 m	Northern	–	–
Landsat 7	ETM+	29 Mar 2010	LE72310962010088EDC00	L1T	30 m	Southern	–	–
Landsat 7	ETM+	16 May 2010	LE72310952010136EDC00	L1T	30 m	Central	–	–

* Processing levels for Landsat were L1T (terrain corrected processing) or L1G (systematic corrected processing). Processing level for ASTER was L1A (reconstructed unprocessed instrument data).

Table 2. Variation in area of the ablation zone for the 52 glacier basins on the eastern side of the SPI (positive values indicate an advance; negative values indicate a retreat). The U70 glacier (ID#30) is excluded from this list because measurement was not possible. N/D = no data.

ID Number (Fig. 1)	Lat/Long	Glacier Name	Total Area (1984/86) (km^2)	Area Change				
				Period 1 (1976/79 to 1984/86) (km^2)	Period 2 (1984/86 to 2000/02) (km^2)	Period 2 (2000/02 to 2008/10) (km^2)	Total (km^2)	Mean Annual Rate ($km^2\,yr^{-1}$)
1	48° 22.666′ S, 73° 25.344′ W	U88	6.61	−0.22	−0.41	−0.15	−0.79	−0.03
2	48° 22.580′ S, 73° 17.974′ W	Lucia	190.88	−1.02	−8.88	−1.36	−11.26	−0.47
3	48° 23.832′ S, 73° 10.010′ W	Pascua	112.39	−0.51	−4.83	−1.50	−6.84	−0.28
4	49° 25.266′ S, 73° 5.731′ W	U87	26.51	−0.47	−0.71	−0.36	−1.55	−0.07
5	48° 30.354′ S, 73° 4.049′ W	Oriental	73.68	−0.47	−1.12	−0.56	−2.15	−0.09
6	48° 35.198′ S, 73° 8.925′ W	Melizo Sur	33.80	−0.27	−0.54	−0.10	−0.91	−0.04
7	48° 36.725′ S, 73° 10.460′ W	U86	6.47	−0.01	−0.06	−0.05	−0.11	0.00
8	48° 37.650′ S, 73° 14.382′ W	Bravo	135.53	−0.78	−1.97	−1.53	−4.28	−0.17
9	48° 40.778′ S, 73° 16.542′ W	U1	8.33	−0.20	0.14	−0.09	−0.15	−0.01
10	48° 42.603′ S, 73° 14.644′ W	U2	12.95	−0.87	−0.24	−0.19	−1.30	−0.05
11	48° 44.982′ S, 73° 13.401′ W	U3	24.85	−0.65	−0.30	−0.49	−1.44	−0.06
12	48° 45.940′ S, 73° 9.256′ W	U85	13.47	−0.22	−0.15	−0.15	−0.52	−0.02
13	48° 47.954′ S, 73° 5.262′ W	U84	11.85	−0.12	−0.26	−0.17	−0.55	−0.02
14	48° 49.984′ S, 73° 8.187′ W	U83	18.47	−0.18	−0.20	−0.11	−0.48	−0.02
15	48° 53.877′ S, 73° 13.813′ W	O'Higgins	807.22	−7.27	−5.56	−2.21	−15.03	−0.60
16	48° 58.913′ S, 73° 9.700′ W	Gaea	29.50	−0.44	−1.26	−0.49	−2.19	−0.09
17	49° 1.318′ S, 73° 10.147′ W	U81	6.93	−0.14	−0.03	0.00	−0.17	−0.01
18	49° 3.758′ S, 73° 6.846′ W	Chico	199.14	−2.13	−2.56	−1.59	−6.27	−0.25
19	49° 6.118′ S, 73° 2.277′ W	Pantoja and Milodon	34.58	−0.95	−0.48	−0.10	−1.53	−0.06
20	49° 9.340′ S, 73° 1.857′ W	Cagliero	10.05	−0.11	−0.03	0.02	−0.12	0.00
21	49° 10.648′ S, 73° 5.462′ W	Gorra Blanca (Sur)	28.44	−0.54	−0.60	−0.18	−1.32	−0.06
22	49° 13.582′ S, 73° 6.960′ W	Marconi	21.44	−0.20	−0.75	−0.22	−1.16	−0.05
23	49° 19.469′ S, 73° 3.361′ W	De Quervain, Rio Tunel, Adela and Torre	58.36	−0.50	−1.79	−0.20	−2.48	−0.10
24	49° 28.181′ S, 73° 9.247′ W	Viedma	1027.81	−4.27	−7.82	−5.78	−17.87	−0.71
25	49° 40.260′ S, 73° 8.494′ W	Moyano	93.90	−2.34	−1.85	−0.99	−5.19	−0.21
26	49° 43.525′ S, 73° 8.715′ W	U73	13.55	−0.14	0.02	0.02	−0.09	0.00

Table 2. Continued.

ID Number (Fig. 1)	Lat/Long	Glacier Name	Total Area (1984/86) (km^2)	Area Change				
				Period 1 (1976/79 to 1984/86) (km^2)	Period 2 (1984/86 to 2000/02) (km^2)	Period 2 (2000/02 to 2008/10) (km^2)	Total (km^2)	Mean Annual Rate ($km^2 yr^{-1}$)
27	49° 44.339′ S, 73° 7.001′ W	U72	0.96	−0.04	0.02	−0.05	−0.08	0.00
28	49° 47.061′ S, 73° 9.962′ W	U71	22.79	−0.22	−0.25	−0.18	−0.65	−0.03
29	49° 53.618′ S, 73° 17.483′ W	Upsala	925.02	−15.12	−35.25	−21.47	−71.84	−2.89
31	49° 57.964′ S, 73° 24.119′ W	U68	13.19	−0.73	−0.45	−0.05	−1.23	−0.05
32	50° 2.470′ S, 73° 22.232′ W	Agassiz	52.61	−0.53	−0.51	−0.30	−1.34	−0.05
33	50° 6.531′ S, 73° 24.580′ W	Onelli and Bolados	76.15	−1.18	−4.19	−3.19	−8.56	−0.34
34	50° 14.698′ S, 73° 21.168′ W	Spegazzini, Peineta and Heim	172.62	−1.56	−0.73	−0.64	−2.93	−0.12
35	50° 19.425′ S, 73° 27.895′ W	U67	19.46	−0.31	−0.22	−0.05	−0.58	−0.02
36	50° 22.906′ S, 73° 27.132′ W	Aguilera	9.59	N/D	−0.02	−0.03	−0.03	0.00
37	50° 23.677′ S, 73° 25.057′ W	Lago Escondida	12.67	−0.37	−0.02	−0.08	−0.47	−0.02
38	50° 24.696′ S, 73° 22.422′ W	Mayo	42.14	−0.65	−0.78	−0.61	−2.04	−0.08
39	50° 25.558′ S, 73° 13.636′ W	Ameghino	101.91	−4.82	−2.25	−0.67	−7.73	−0.31
40	50° 30.222′ S, 73° 9.301′ W	Perito Moreno	265.39	−1.79	−1.44	0.61	−2.61	−0.10
41	50° 34.401′ S, 73° 7.783′ W	U64	7.05	−0.09	−0.41	0.02	−0.47	−0.02
42	50° 42.141′ S, 73° 6.116′ W	Frias and Grande	63.80	−3.42	−2.75	−1.71	−7.87	−0.34
43	50° 46.763′ S, 73° 11.324′ W	Dickson/Cubo	76.95	−4.83	−6.18	−1.43	−12.44	−0.49
44	50° 56.514′ S, 73° 15.498′ W	Grey	280.93	−2.18	−8.87	−3.97	−15.02	−0.60
45	50° 56.646′ S, 73° 19.520′ W	U63	2.79	−0.11	−0.07	0.00	−0.18	−0.01
46	50° 59.069′ S, 73° 21.985′ W	Pingo	61.74	−1.02	−0.85	−1.57	−3.44	−0.14
47	51° 1.931′ S, 73° 23.253′ W	U62	12.76	−0.53	−0.45	−0.21	−1.18	−0.05
48	51° 11.361′ S, 73° 18.398′ W	Tyndall	329.54	−5.48	−10.37	−12.34	−28.20	−1.16
49	51° 12.130′ S, 73° 25.390′ W	U61	13.15	−0.84	−1.13	−0.11	−2.08	−0.09
50	51° 14.751′ S, 73° 25.352′ W	U60	16.81	−1.22	−0.74	−1.28	−3.24	−0.15
51	51° 19.574′ S, 73° 22.840′ W	U59	11.27	−1.23	−0.27	−0.33	−1.83	−0.08
52	51° 22.516′ S, 73° 20.642′ W	Balmaceda	70.13	−1.37	−3.09	−2.81	−7.27	−0.30
53	51° 24.212′ S, 73° 21.041′ W	U58	9.67	−0.06	−0.36	−0.08	−0.50	−0.02

Table 3. Variation in area of the ablation zone for the 78 glacier basins on the western side of the SPI (positive values indicate an advance; negative values indicate a retreat). The U47 (ID#68), U19 (ID#105), U16 (ID#107), U17 (ID#108), U93 (ID#126), U9 (ID#129), U89 (ID#137), and U94 (ID#138) glaciers are excluded from this list because they were not measured. N/D = No data.

ID Number (Fig. 1)	Lat/Long	Glacier Name	Total Area (1984/86) (km^2)	Area Change				
				Period 1 (1976/79 to 1984/86) (km^2)	Period 2 (1984/86 to 2000/02) (km^2)	Period 2 (2000/02 to 2008/10) (km^2)	Total (km^2)	Mean Annual Rate ($km^2 yr^{-1}$)
54	51° 25.323′ S, 73° 27.493′ W	U57	11.06	−0.82	−0.09	−0.14	−1.06	−0.04
55	51° 25.349′ S, 73° 29.537′ W	U56	3.77	N/D	−0.05	−0.03	−0.03	0.00
56	51° 24.210′ S, 73° 30.392′ W	U55	14.02	0.00	−0.46	−0.22	−0.22	−0.01
57	51° 21.605′ S, 73° 31.651′ W	Snowy	22.03	−0.38	−2.88	−0.66	−3.92	−0.16
58	51° 20.190′ S, 73° 28.481′ W	U54	22.83	−0.48	−0.53	−0.05	−1.06	−0.05
59	51° 16.951′ S, 73° 30.067′ W	U53	5.04	−0.07	−0.09	−0.12	−0.29	−0.02
60	51° 16.604′ S, 73° 32.982′ W	HPS41	76.44	−0.60	−2.67	−4.60	−7.87	−0.36
61	51° 2.370′ S, 73° 38.700′ W	HPS38	155.75	N/D	−8.75	−3.48	−3.48	−0.16
62	50° 59.493′ S, 73° 41.417′ W	U51	59.25	N/D	−5.70	−2.84	−2.84	−0.11
63	50° 55.984′ S, 73° 39.240′ W	Amalia	172.87	N/D	−2.25	−0.24	−0.24	−0.01
64	50° 52.814′ S, 73° 38.725′ W	U50	2.74	N/D	−0.17	−0.06	−0.06	0.00
65	50° 49.502′ S, 73° 42.000′ W	Asia	127.96	N/D	−2.73	−0.17	−0.17	−0.01
66	50° 46.516′ S, 73° 40.772′ W	U49	21.65	N/D	−0.93	−0.32	−0.32	−0.01
67	50° 43.897′ S, 73° 40.997′ W	U48	20.88	N/D	−1.30	−0.48	−0.48	−0.02
69	50° 41.206′ S, 73° 34.984′ W	U46	33.72	N/D	−0.30	−0.40	−0.40	−0.02
70	50° 43.264′ S, 73° 30.877′ W	HPS34	163.75	N/D	−0.44	−0.40	−0.40	−0.02
71	50° 41.301′ S, 73° 25.019′ W	U45	17.99	N/D	0.12	−0.03	−0.03	0.00
72	50° 41.313′ S, 73° 19.031′ W	Calvo	113.22	N/D	0.04	0.02	0.02	0.00
73	50° 38.276′ S, 73° 25.875′ W	U44	22.62	N/D	−0.02	0.06	0.06	0.00
74	50° 36.718′ S, 73° 31.352′ W	HPS31	161.55	N/D	−0.46	−0.10	−0.10	0.00
75	50° 33.416′ S, 73° 36.222′ W	U43	46.40	N/D	−0.78	−0.29	−0.29	−0.01
76	50° 31.538′ S, 73° 36.879′ W	U42	14.66	N/D	−0.47	−0.08	−0.08	0.00
77	50° 28.926′ S, 73° 32.446′ W	HPS29	87.60	N/D	−1.66	−0.01	−0.01	0.00
78	50° 27.638′ S, 73° 31.685′ W	U41	2.37	N/D	−0.03	−0.02	−0.02	0.00

Table 3. Continued.

ID Number (Fig. 1)	Lat/Long	Glacier Name	Total Area (1984/86) (km^2)	Area Change: Period 1 (1976/79 to 1984/86) (km^2)	Area Change: Period 2 (1984/86 to 2000/02) (km^2)	Area Change: Period 2 (2000/02 to 2008/10) (km^2)	Area Change: Total (km^2)	Area Change: Mean Annual Rate ($km^2\ yr^{-1}$)
79	50° 26.951′ S, 73° 30.455′ W	HPS28	46.25	N/D	−0.74	−0.02	−0.02	0.00
80	50° 24.741′ S, 73° 30.074′ W	U40	16.92	N/D	−0.57	−0.17	−0.17	−0.01
81	50° 21.093′ S, 73° 31.288′ W	HPS27	39.73	N/D	−0.47	−0.11	−0.11	0.00
82	50° 20.624′ S, 73° 34.649′ W	U38	26.20	N/D	−0.27	−0.60	−0.60	−0.02
83	50° 22.131′ S, 73° 43.350′ W	U37	36.14	N/D	−1.02	−0.42	−0.42	−0.02
84	50° 25.237′ S, 73° 46.869′ W	U36	8.05	N/D	−0.34	−0.11	−0.11	0.00
85	50° 28.567′ S, 73° 47.384′ W	U35	18.12	N/D	−0.24	−0.26	−0.26	−0.01
86	50° 25.976′ S, 73° 53.605′ W	U34	46.71	−1.04	−2.86	−0.85	−4.75	−0.19
87	50° 23.280′ S, 73° 52.468′ W	U33	1.57	N/D	−0.07	0.00	0.00	0.00
88	50° 22.695, 73° 51.482′ W	U32	5.26	N/D	−0.45	−0.05	−0.05	0.00
89	50° 21.202′ S, 73° 52.467′ W	Guilardi	176.98	−0.04	−0.56	−0.25	−0.86	−0.04
90	50° 17.900′ S, 73° 48.903′ W	Europa	408.68	−1.32	−0.02	−0.08	−1.42	−0.06
91	50° 15.684′ S, 73° 51.052′ W	U31	5.20	−0.19	0.00	−0.11	−0.29	−0.01
92	50° 14.544′ S, 73° 52.126′ W	U30	12.10	−0.38	−0.42	−0.09	−0.89	−0.04
93	50° 14.405′ S, 73° 54.272′ W	U29	3.96	0.01	−0.11	−0.02	−0.12	0.00
94	50° 12.483′ S, 73° 53.818′ W	U28	14.05	−0.09	0.02	−0.02	−0.09	0.00
95	50° 10.391′ S, 73° 52.324′ W	U27	23.97	−0.35	−0.70	−0.15	−1.20	−0.05
96	50° 8.616′ S, 73° 53.907′ W	U26	21.26	−0.54	−0.73	−0.31	−1.58	−0.06
97	50° 6.833′ S, 73° 54.694′ W	U25	8.75	−0.22	−0.32	−0.03	−0.57	−0.02
98	50° 5.544′ S, 73° 53.580′ W	U24	5.26	−0.15	−0.09	0.02	−0.22	−0.01
99	50° 3.632′ S, 73° 54.866′ W	U23	5.74	−0.09	−0.29	−0.07	−0.44	−0.02
100	50° 4.212′ S, 73° 51.972′ W	Penguin	468.24	−2.55	0.14	−0.05	−2.46	−0.10
101	50° 1.091′ S, 73° 49.962′ W	U22	20.88	−0.42	−0.46	−0.19	−1.07	−0.04
102	49° 58.575′ S, 73° 50.915′ W	HPS19	173.95	−0.53	0.07	0.01	−0.45	−0.02
103	49° 56.912′ S, 73° 50.756′ W	U21	10.01	−0.09	−0.05	−0.04	−0.18	−0.01
104	49° 53.145′ S, 73° 48.175′ W	U20	50.73	−0.92	0.12	−0.60	−1.39	−0.06
106	49° 49.660′ S, 73° 46.581′ W	U18	67.19	−0.51	−0.57	−0.05	−1.13	−0.05

Table 3. Continued.

ID Number (Fig. 1)	Lat/Long	Glacier Name	Total Area (1984/86) (km^2)	Area Change: Period 1 (1976/79 to 1984/86) (km^2)	Area Change: Period 2 (1984/86 to 2000/02) (km^2)	Area Change: Period 2 (2000/02 to 2008/10) (km^2)	Area Change: Total (km^2)	Area Change: Mean Annual Rate ($km^2\ yr^{-1}$)
109	49° 46.308′ S, 73° 47.011′ W	U15	42.68	N/D	−1.32	−0.76	−2.08	−0.08
110	49° 45.533′ S, 73° 43.280′ W	U14	17.22	−0.78	0.17	0.02	−0.59	−0.02
111	49° 47.033′ S, 73° 37.464′ W	HPS15	193.16	−0.30	0.00	0.07	−0.23	−0.01
112	49° 43.659′ S, 73° 37.609′ W	HPS13	143.19	−0.44	−0.11	0.05	−0.50	−0.02
113	49° 36.630′ S, 73° 40.709′ W	HPS12	206.04	−1.83	−8.99	−6.14	−16.96	−0.70
114	49° 31.622′ S, 73° 44.576′ W	HPS10	98.96	−1.03	−0.52	−0.89	−2.43	−0.10
115	49° 25.726′ S, 73° 43.600′ W	U13	43.87	0.47	2.68	0.60	3.76	0.16
116	49° 23.377′ S, 73° 42.808′ W	U12	3.30	−0.01	−0.08	−0.02	−0.11	0.00
117	49° 9.109′ S, 73° 56.289′ W	Pio XI	1278.50	4.70	8.64	4.85	18.19	0.75
118	49° 2.987′ S, 73° 42.266′ W	HPS09	59.09	−0.58	−3.20	−3.92	−7.70	−0.31
119	48° 59.996′ S, 73° 37.970′ W	U11	12.38	−0.94	0.01	−0.09	−1.02	−0.05
120	49° 0.386′ S, 73° 41.021′ W	HPS08	50.80	−1.01	−5.04	−0.16	−6.20	−0.26
121	48° 57.357′ S, 73° 44.645′ W	U10	37.64	−0.59	−1.60	−0.08	−2.27	−0.10
122	48° 57.402′ S, 73° 52.072′ W	Greve	526.41	−5.19	−18.59	−8.42	−32.20	−1.33
123	48° 50.899′ S, 74° 1.084′ W	Occidental	185.26	−7.43	−7.48	−8.11	−23.02	−0.98
124	48° 43.151′ S, 73° 56.983′ W	Tempano	291.09	−9.37	−7.33	−3.84	−20.55	−0.88
125	48° 38.426′ S, 73° 51.050′ W	Bernardo	584.67	−3.01	−20.02	−5.26	−28.28	−1.23
127	48° 33.960′ S, 73° 47.298′ W	U92	68.42	−3.39	−3.23	−4.43	−11.06	−0.50
128	48° 31.130′ S, 73° 45.777′ W	U91	2.33	−0.20	−0.20	−0.04	−0.44	−0.02
130	48° 29.816′ S, 73° 45.520′ W	U8	7.84	−0.26	−0.64	−0.17	−1.08	−0.05
131	48° 27.136′ S, 73° 46.066′ W	Ofhidro	110.67	−0.85	−3.06	−2.29	−6.19	−0.26
132	48° 25.893′ S, 73° 43.454′ W	U90	2.46	−0.31	−0.60	−0.05	−0.97	−0.04
133	48° 26.456′ S, 73° 40.706′ W	U7	5.51	−0.19	−0.37	−0.17	−0.73	−0.03
134	48° 24.121′ S, 73° 39.513′ W	U6	5.74	−0.46	−0.40	−0.10	−0.96	−0.04
135	48° 22.338′ S, 73° 40.183′ W	U5	9.63	−0.04	0.02	−0.11	−0.13	−0.01
136	48° 20.552′ S, 73° 37.784′ W	U4	19.16	−0.10	−0.34	−0.16	−0.61	−0.03
139	48° 20.896′ S, 73° 29.284′ W	Jorge Montt	505.49	−2.45	−41.48	−9.82	−53.75	−2.33

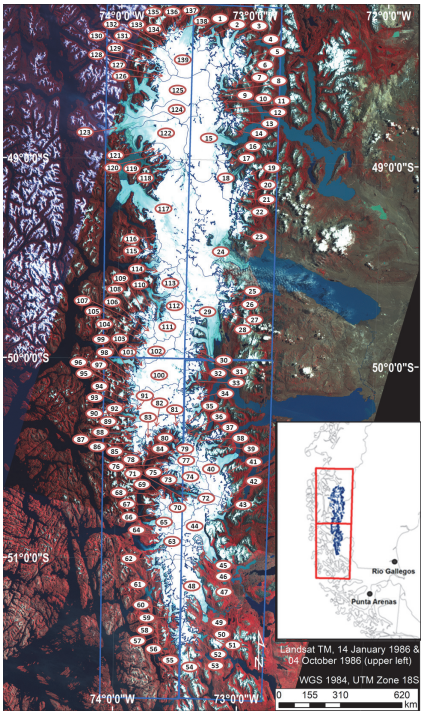

Fig. 1. Landsat TM mosaic (14 January 1986 and 4 October 1986; RGB = 742) of the SPI with labels for each glacier in the study (see Tables 2 and 3). Blue boxes indicate the quadrants used to separate the SPI into four sub-study areas: northeast, northwest, southeast and southwest. Inset: location of the study area in Chile and Argentina; red trapezoids indicate location of climate reanalysis cells used in this study.

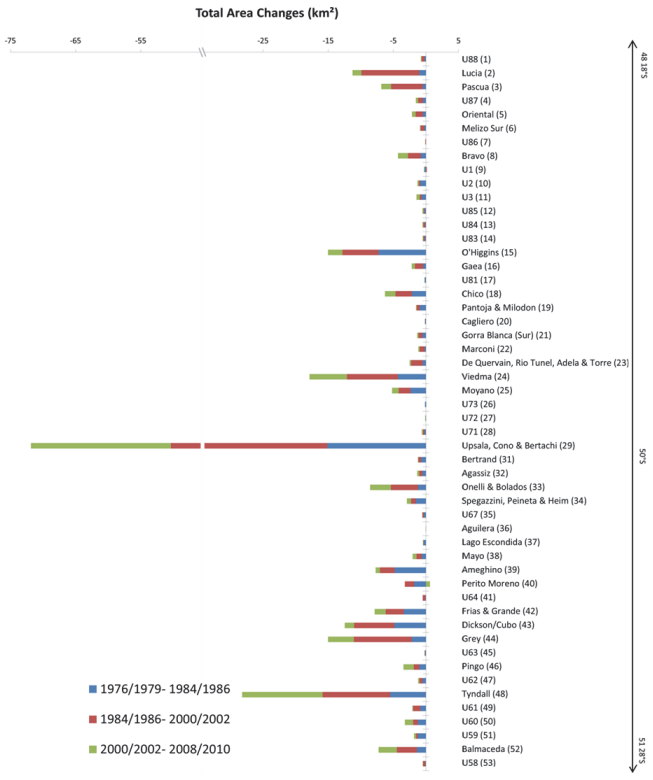

Fig. 2. Total area change of glaciers on the eastern side of the SPI (1976/79–2008/10).

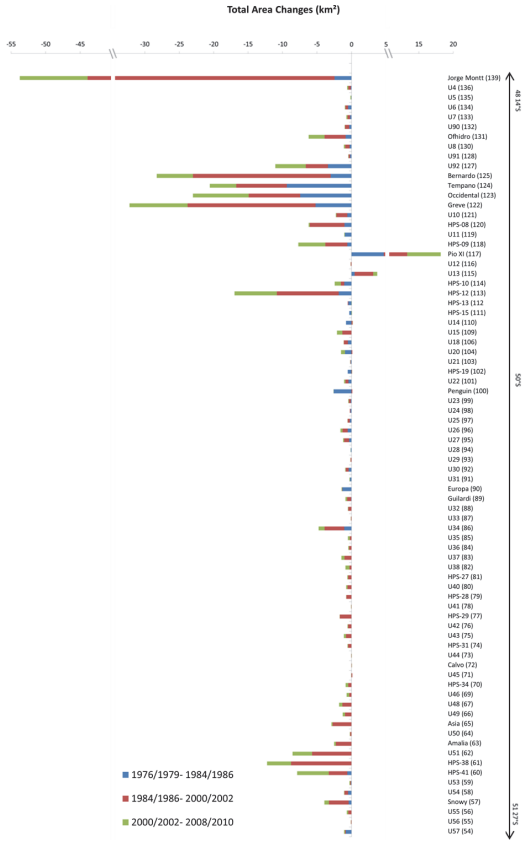

Fig. 3. Total area change of glaciers on the western side of the SPI (1976/79–2008/10).

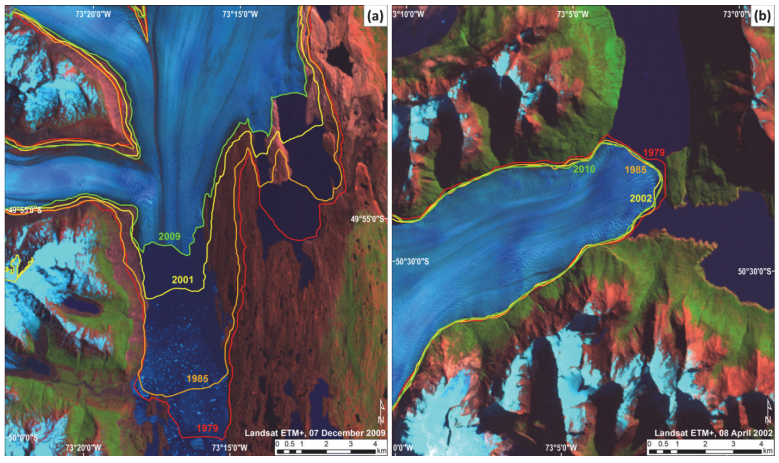

Fig. 4. Area changes of the ablation zone of two glaciers on the eastern side of the SPI: **(a)** Landsat ETM+ image (7 December 2009; RGB = 742) of the Upsala Glacier and **(b)** Landsat ETM+ image (8 April 2002; RGB = 742) of the Perito Moreno Glacier.

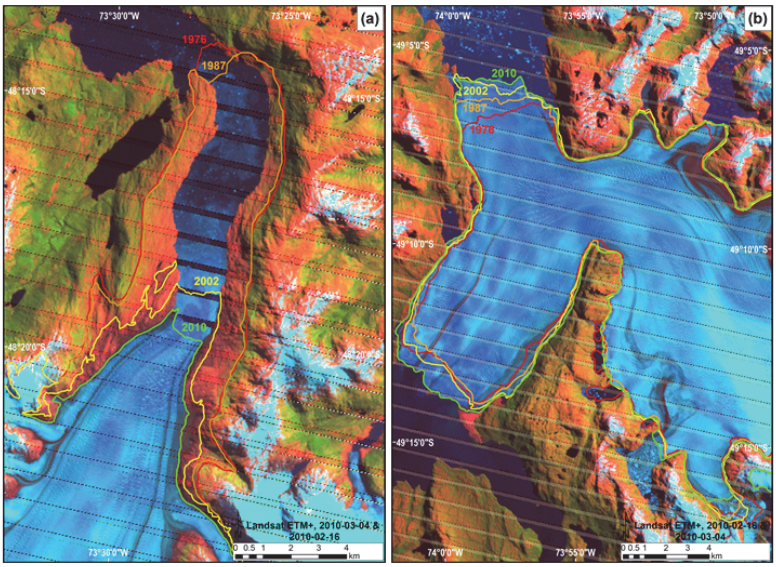

Fig. 5. Area changes of the ablation zone of two glaciers on the western side of the SPI: **(a)** Landsat ETM+ image (4 March 2010 and 16 February 2010; RGB = 742) of the Jorge Montt Glacier and **(b)** Landsat ETM+ image (16 February 2010 and 4 March 2010; RGB = 742) of the Pio XI Glacier. Note the striping in the Landsat ETM+ imagery due to the failure of the scan-line corrector; to fill gaps the original image was superimposed over a Landsat scene acquired within a year of the original.

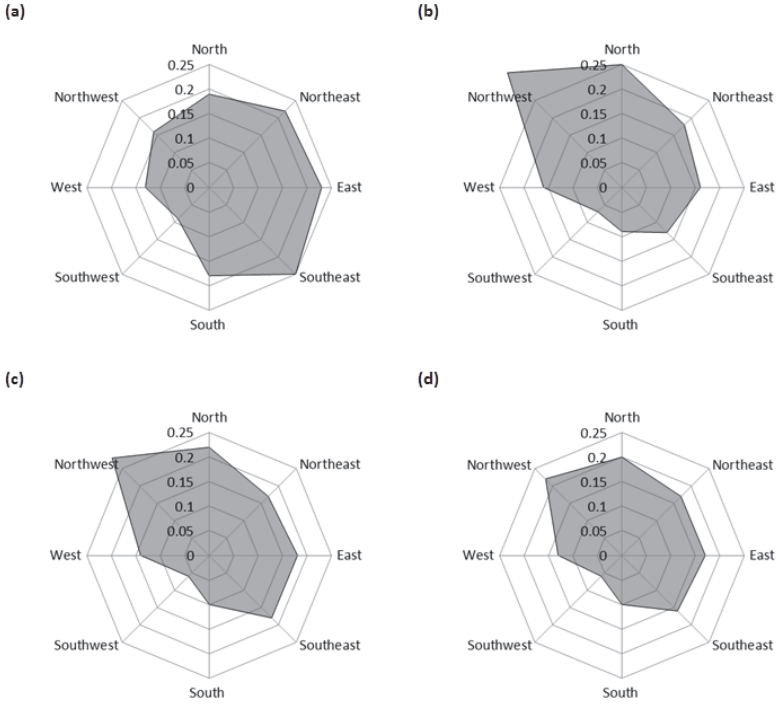

Fig. 6. Radar graphs illustrating the distribution of mean annual areal retreat rates ($km^2\ yr^{-1}$) for each quadrant and study period (excluding glaciers which advanced): **(a)** 1976/79 to 1984/86; **(b)** 1984/86 to 2000/02; **(c)** 2000/02 to 2008/10; **(d)** 1976/79 to 2008/10.

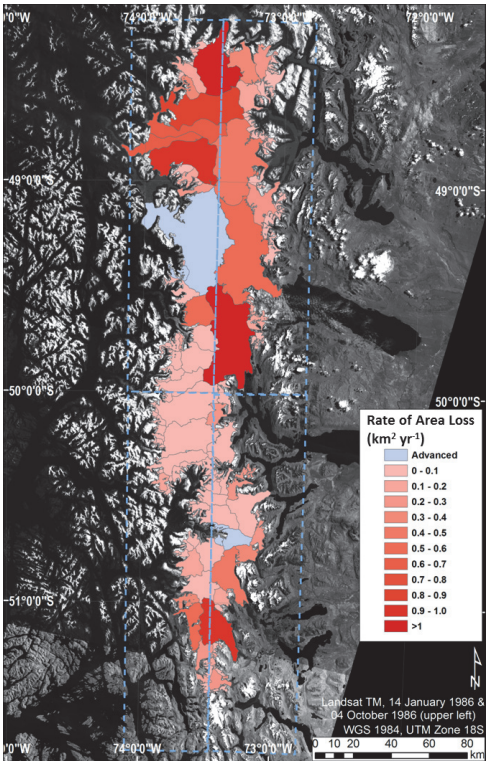

Fig. 7. Distribution of long-term changes for every glacier basin across the SPI from 1976/79 to 2008/10 (for 108 basins), and 1984/86 to 2008/10 (for 30 basins, due to lack of cloud-free images in the 1970s). Blue boxes indicate the quadrants used to separate the SPI into four sub-study areas: northeast, northwest, southeast and southwest.

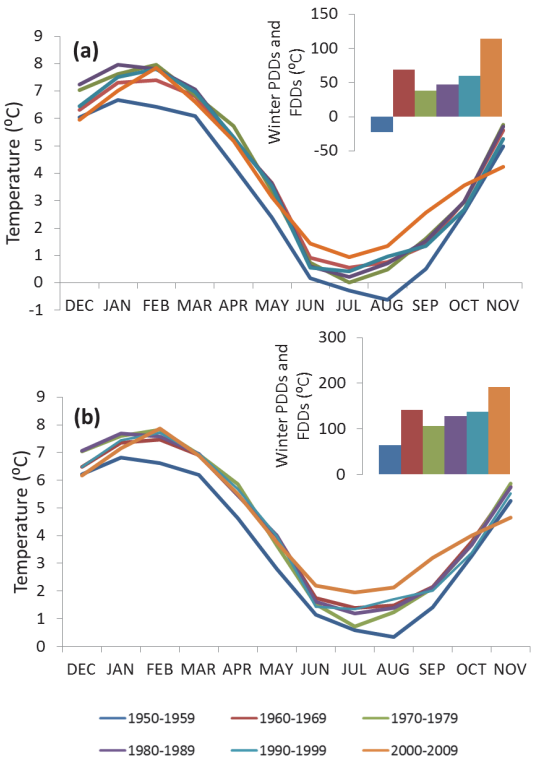

Fig. 8. Decadal surface temperature patterns derived from NCEP/NCAR climate reanalysis from 1959 to 2010 for: **(a)** northern half of the SPI; **(b)** southern half of the SPI. Inset graphs show changes in winter (June, July, August) PDDs and FDDs calculated from monthly data. See Fig. 1 inset for grid positions.